

Coulomb interaction unlocks Majorana-mediated electron teleportation between Quantum dots

Sirui Yu,¹ Hong Mao,¹ Jinshuang Jin,^{1,*} and Chui-Ping Yang¹

¹*School of Physics, Hangzhou Normal University, Hangzhou, Zhejiang 311121, China*

(Dated: March 5, 2026)

We investigate quantum transport in a hybrid system composed of two quantum dots (QDs) coupled through a pair of spatially separated Majorana zero modes (MZMs) with negligible coupling energy. We focus on nonlocal correlations mediated by the MZMs, particularly the role of Coulomb interaction U between the QDs and the Majorana wire. Using the numerically exact fermionic dissipation equation of motion (DEOM) method, we compute both the transient current and the current-current cross-correlation noise spectrum. In the non-interacting case ($U = 0$), destructive interference between the degenerate normal tunneling and anomalous tunneling channels suppresses electron teleportation between the dots. Introducing a finite Coulomb interaction U lifts this channel degeneracy, enabling strong nonlocal correlations and inter-dot electron teleportation. This effect manifests as a robust signal in the cross-correlation noise spectrum, which is significantly stronger than that induced by a finite Majorana coupling energy ε_M . Our findings propose Coulomb interaction as an efficient and experimentally accessible control parameter for generating and detecting Majorana-mediated nonlocal transport in the topologically relevant long-wire limit ($\varepsilon_M \rightarrow 0$).

PACS numbers:

I. INTRODUCTION

The pursuit of topological quantum computation has stimulated intense interest in Majorana zero modes (MZMs), as evidenced by extensive theoretical [1–13] and experimental [14–18] studies. MZMs are exotic quasiparticles obeying non-Abelian statistics, predicted to emerge at the ends of one-dimensional topological superconducting nanowires [2, 3]. Their nonlocal nature, manifested as spatially separated zero-energy states, offers a promising platform for fault-tolerant quantum information processing [19–22]. A key signature of this nonlocality is electron teleportation [23–25], whereby an electron is coherently transferred between distant points via MZMs without direct overlap of the electronic wavefunctions.

A common approach for demonstrating nonlocality involves the measurement of nonlocal current cross-correlations [4–13]. Previous work have shown that a finite Majorana coupling energy (ε_M) can generate non-zero cross-correlation noise. However, this noise vanishes in the limit $\varepsilon_M \rightarrow 0$, both for MZMs coupled directly to leads [7–9] and for MZMs coupled via QDs (referred to as a QD-MZM system) [10–13], as illustrated in Fig. 1. Notably, Feng *et al.*, [13] clarified that the absence of cross-correlation at $\varepsilon_M \rightarrow 0$ stems from a degeneracy of between the Andreev process and the ‘teleportation’, channels. They proposed lifting this degeneracy by introducing finite charging energy E_C on the Majorana island, which restores nonzero cross-correlation even in the $\varepsilon_M \rightarrow 0$ limit within the QD-MZM transport geometry [13]. This work generalizes Ref. [25], where a large E_C limit was suggested to fully suppress the Andreev

process, thereby isolating a pure electron ‘teleportation’ channel alone for MZMs coupled directly to leads. The role of large E_C in restoring cross-correlation noise at $\varepsilon_M \rightarrow 0$ has also been demonstrated in Ref. [12]. Furthermore, nonlocal properties arising from finite ε_M (via shorter wires) or a finite/large charging energy E_C have been proposed to generate entanglement between QDs [26–29] or nanomechanical oscillators [30]. Nevertheless, ε_M is inherently small in long wires, which are desirable for topological protection, and experimental detection of nonlocal correlations remains elusive.

In this work, we propose and theoretically demonstrate that Coulomb interaction between the QDs and the Majorana wire provides an efficient and experimentally viable alternative mechanism to realize the electron teleportation between two well-separated QDs mediated by MZMs in a long topological wire ($\varepsilon_M \rightarrow 0$). As revealed in Ref. [31], Coulomb interaction between the QD and the superconducting section induces an additional overlap of the wave functions describing the individual MZMs, even when they are spatially distant. For InAs systems, the interaction strength U is estimated to range from μeV to meV , depending on the size of the QD formed at the bare region nanowire [31].

Reanalyzing the intrinsic transport mechanism for the hybrid QD-MZM system (Fig. 1), we find that it is described by two distinct quantum tunneling processes: normal tunneling (NT) and anomalous tunneling (AT). These are associated with electron (ε_M) and hole ($-\varepsilon_M$) transport channels via the Majorana fermionic mode, respectively. In the ideal long-wire limit ($\varepsilon_M \rightarrow 0$), these two tunneling channels become degenerate. This degeneracy causes destructive quantum interference between the NT and AT paths, suppressing the coherent transfer of electrons between the dots and eliminating nonlocal cross-correlations. We show that Coulomb in-

*Electronic address: jsjin@hznu.edu.cn

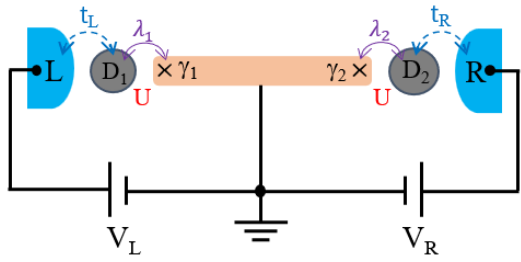


FIG. 1: Schematic of the transport setup for a hybrid quantum dot-Majorana zero mode (QD-MZM) system. Two QDs are coupled to a pair of Majorana modes (γ_1 and γ_2), located at the ends of a superconducting nanowire, with coupling strengths λ_1 and λ_2 , respectively. Each QD is contacted by an electron reservoirs via tunneling amplitudes t_L and t_R .

interaction between QDs and Majorana wire breaks this channel degeneracy, thereby unlocking robust Majorana-mediated electron teleportation. Using the numerically exact fermionic dissipation equation of motion (DEOM) method, we investigate quantum transport through the QD-MZM structure (Fig. 1). We compute both transient currents $I(t)$ and the current-current cross-correlation noise spectrum $S_{LR}(\omega)$, presenting their characteristic features in detail.

This paper is organized as follows. In Sec. II, we describe the model Hamiltonian and outline the DEOM methodology for accurate quantum transport calculations. Section III analyzes the isolated hybrid QD-MZM system, contrasting the non-interacting and interacting cases to elucidate the role of U in establishing inter-dot correlations. In Sec. IV, we present numerical results for transport currents and the cross-correlation noise spectrum, demonstrating how Coulomb interaction generates measurable teleportation signatures. Finally, we summarize our findings in Sec. V.

II. METHODOLOGY

A. Model description

The system under study, illustrated in Fig. 1, consists of two quantum dots (QDs) coupled via a pair of Majorana zero modes (MZMs), γ_1 and γ_2 , located at the ends of a topological superconducting nanowire. Each QD is also connected to an individual normal electron reservoir. The total Hamiltonian comprises three parts, $H_{\text{tot}} = H_B + H_{\text{SB}} + H_S$. The first part is the bath referring to the two electron reservoirs (L and R), which is given by $H_B = \sum_{\alpha} \varepsilon_{\alpha k} \hat{c}_{\alpha k}^{\dagger} \hat{c}_{\alpha k}$, with $\alpha = L, R$. The system-bath coupling Hamiltonian (H_{SB}) describes the standard electrons tunneling between the QDs and electrodes:

$$H_{\text{SB}} = \sum_{\alpha k u} (t_{\alpha k u} \hat{a}_u^{\dagger} \hat{c}_{\alpha k} + \text{H.c.}), \quad (1)$$

where \hat{a}_u^{\dagger} (\hat{a}_u) is the electron creation (annihilation) operator in the QD- u . Throughout this work, we set $e = \hbar = 1$, for the electron charge and the Planck constant.

The central system is described by $H_S = H_0 + H' + H_U$, which includes the bare Hamiltonian (H_0) of the dots and MZMs, the QD-MZM coupling (H'), and Coulomb interaction between the electrons of the QDs and the Majorana wire (H_U). Within the low-energy effective description, these terms are given by [11, 13, 31, 32],

$$H_0 = \sum_{u=1,2} \varepsilon_u \hat{a}_u^{\dagger} \hat{a}_u + \frac{i}{2} \varepsilon_M \hat{\gamma}_1 \hat{\gamma}_2, \quad (2a)$$

$$H' = \sum_{u=1,2} \lambda_u (\hat{a}_u^{\dagger} - \hat{a}_u) \hat{\gamma}_u, \quad (2b)$$

$$H_U = \sum_{u=1,2} U_u \hat{n}_u \hat{n}_M, \quad (2c)$$

where each QDs is modeled by a single fermionic mode with creation (annihilation) operator \hat{a}_u^{\dagger} (\hat{a}_u) and energy level ε_u . The coupling energy ε_M between the two MZMs $\hat{\gamma}_1$ and $\hat{\gamma}_2$ depends on the wire length. The parameters λ_u and U_u denote, respectively, the coupling coefficients and the Coulomb interaction between the QD- u and the Majorana wire. Here, $\hat{n}_u = \hat{a}_u^{\dagger} \hat{a}_u$ and $\hat{n}_M = \hat{f}^{\dagger} \hat{f}$ are the occupation operators of the dots and wires, respectively.

The Majorana operators can be expressed in terms of regular fermionic operators via $\hat{\gamma}_1 = \hat{f} + \hat{f}^{\dagger}$ and $\hat{\gamma}_2 = -i(\hat{f} - \hat{f}^{\dagger})$, where \hat{f}^{\dagger} (\hat{f}) is the fermionic creation (annihilation) operator. In this representation, the Hamiltonian Eq. (2) becomes

$$H_0 = \sum_{u=1,2} \varepsilon_u \hat{a}_u^{\dagger} \hat{a}_u + (\varepsilon_M - \frac{1}{2}) \hat{f}^{\dagger} \hat{f}, \quad (3a)$$

$$H' = \sum_{u=1,2} \lambda_u [\hat{a}_u^{\dagger} \hat{f} + (-)^u \hat{a}_u^{\dagger} \hat{f}^{\dagger} + \text{H.c.}], \quad (3b)$$

$$H_U = \sum_{u=1,2} \frac{1}{2} U_u \hat{n}_u (i \hat{\gamma}_1 \hat{\gamma}_2 + 1). \quad (3c)$$

In this form, the coupling H' between QDs and MZMs consists of two distinct processes: the normal tunneling (NT) term, given by $\lambda[\hat{a}_u^{\dagger} \hat{f} + \text{H.c.}]$, and anomalous tunneling (AT) term, given by $\lambda[\hat{a}_u^{\dagger} \hat{f}^{\dagger} + \text{H.c.}]$. Notably, the structure of H_U closely resembles the term $\varepsilon_M \hat{\gamma}_1 \hat{\gamma}_2$ in H_0 Eq. (2a). Therefore, the QD-MZM Coulomb interaction leads to additional hybridization of the Majorana modes, whose amplitude $\frac{1}{2} U_u \hat{n}_u$ depends on occupancy of the QD- u . As shown below, this has a dramatic effect on Majorana-mediated electron teleportation between the two QDs.

B. The DEOM approach

In this work, we employ the established fermionic dissipation equation of motion (DEOM) method for accurate

evaluations on the transport current and its noise spectrum [33–35]. The core idea of DEOM is the introduction of the *dissipatons*, quasi-particles used to decompose the bath operators:

$$\tilde{F}_{\alpha u}^{\sigma} \equiv -\sigma \hat{F}_{\alpha u}^{\sigma} \equiv \sum_{m=1}^M \hat{f}_{\alpha u m}^{\sigma}, \quad (4)$$

where $\hat{F}_{\alpha u}^{\bar{\sigma}} = \sum_k t_{\alpha u k} c_{\alpha k} = (\hat{F}_{\alpha u}^{\sigma})^{\dagger}$ and $\sigma = +, -$ (with $\bar{\sigma}$ denoting the opposite sign) identifies the creation/annihilation operators. The system-reservoir coupling in Eq. (1) can then be expressed as

$$H_{\text{SB}} = \sum_{\alpha u \sigma} \hat{a}_u^{\bar{\sigma}} \tilde{F}_{\alpha u}^{\sigma} = \sum_{\alpha u \sigma m} \hat{a}_u^{\bar{\sigma}} \hat{f}_{\alpha u m}^{\sigma}. \quad (5)$$

Within the fluctuation-dissipation framework, the bath correlation function $\langle \hat{F}_{\alpha u}^{\sigma}(t) \hat{F}_{\alpha v}^{\bar{\sigma}}(0) \rangle_{\text{B}} = \frac{1}{\pi} \int_{-\infty}^{\infty} d\omega e^{i\omega t} J_{\alpha uv}^{\sigma}(\omega) f_{\alpha}^{\sigma}(\omega)$ is considered for a Lorentzian hybridization spectral function,

$$J_{\alpha uv}(\omega) \equiv \pi \sum_k t_{\alpha k} t_{\alpha k}^* \delta(\omega - \varepsilon_{\alpha k}) = \frac{\Gamma_{\alpha uv} W^2}{\omega^2 + W^2}. \quad (6)$$

Here $J_{\alpha uv}(\omega) = J_{\alpha vu}^{-}(\omega) = J_{\alpha uv}^{+}(\omega)$, and $f_{\alpha}^{+}(\omega) = 1 - f_{\alpha}^{-}(\omega)$ is the Fermi distribution function. Using an optimal Padé spectrum decomposition of the Fermi function [36, 37], the bath correlation function can be written in exponential form,

$$\langle \hat{F}_{\alpha u}^{\sigma}(t) \hat{F}_{\alpha v}^{\bar{\sigma}}(0) \rangle_{\text{B}} = \sum_{m=1}^M \eta_{\alpha uv m}^{\sigma} e^{-\gamma_{\alpha m}^{\sigma} t}, \quad (7)$$

which leads to

$$\langle \hat{f}_{\alpha u m}^{\sigma}(t) \hat{f}_{\alpha' v m'}^{\bar{\sigma}'}(0) \rangle_{\text{B}} = -\delta_{\sigma \bar{\sigma}'} \delta_{\alpha \alpha'} \delta_{m m'} \eta_{\alpha uv m}^{\sigma} e^{-\gamma_{\alpha m}^{\sigma} t}.$$

Introducing the composite index $j \equiv (\sigma \alpha u m)$ and $\bar{j} \equiv (\bar{\sigma} \alpha' v m')$, the dynamical variables in DEOM are the reduced dissipaton density operators (DDOs):

$$\rho_j^{(n)}(t) \equiv \rho_{j_1 \dots j_n}^{(n)}(t) \equiv \text{tr}_{\text{B}} \left[(\hat{f}_{j_n} \dots \hat{f}_{j_1})^{\circ} \rho_{\text{tot}}(t) \right], \quad (8)$$

where the product inside the circled $(\dots)^{\circ}$ is *irreducible*.

From the perspective of quantum dissipation theory, the central QD-MZM hybrid system is described by the reduced system density operator $\rho(t) \equiv \text{tr}_{\text{B}}[\rho_{\text{tot}}(t)]$. Taking the time derivative and tracing over the reservoirs leads to the the DEOM (equivalent to the hierarchical equations of motion, HEOM) [33–35],

$$\begin{aligned} \dot{\rho}_j^{(n)}(t) = & - \left(i\mathcal{L}_s + \sum_{r=1}^n \gamma_{j_r} \right) \rho_j^{(n)}(t) - i \sum_j \mathcal{A}_{\bar{j}j} \rho_{\bar{j}j}^{(n+1)}(t) \\ & - i \sum_{r=1}^n (-)^{n-r} \mathcal{C}_{j_r} \rho_{\bar{j}_r}^{(n-1)}(t), \end{aligned} \quad (9)$$

where, $\mathcal{L}_s(\cdot) = [H_s, (\cdot)]$ and the superoperators, $\mathcal{A}_{\bar{j}} \equiv \mathcal{A}_{\alpha u m}^{\bar{\sigma}} = \mathcal{A}_u^{\bar{\sigma}}$ and $\mathcal{C}_j \equiv \mathcal{C}_{\alpha u m}^{\sigma}$ are defined via

$$\begin{aligned} \mathcal{A}_u^{\sigma} \hat{O}_{\pm} & \equiv a_u^{\sigma} \hat{O}_{\pm} \pm \hat{O}_{\pm} \hat{a}_u^{\sigma} \equiv [\hat{a}_u^{\sigma}, \hat{O}_{\pm}]_{\pm}, \\ \mathcal{C}_{\alpha u m}^{\sigma} \hat{O}_{\pm} & \equiv \sum_v (\eta_{\alpha uv m}^{\sigma} \hat{a}_v^{\sigma} \hat{O}_{\pm} \mp \eta_{\alpha uv m}^{\bar{\sigma}*} \hat{O}_{\pm} \hat{a}_m^{\sigma}), \end{aligned} \quad (10)$$

with \hat{O}_{\pm} denoting an arbitrary operator of even (+) or odd (−) fermionic parity. The reduced system density operator is $\rho(t) \equiv \text{tr}_{\text{B}} \rho_{\text{tot}}(t) = \rho^{(0)}(t)$. All higher-tier DDOs $\{\rho_j^{(n \geq 1)}\}$ captures entangled system–bath dynamics and are physically well-defined in Eq. (8).

The DEOM provides a unified framework for both non-interacting and interacting open quantum systems. For noninteracting systems, the hierarchy terminates exactly at tier $L = 2$. In fact, truncating at $L = 2$ yields an exact equation for the single-particle density matrix, $\rho_{uv} = \text{tr}_s[a_v^{\dagger} a_u \rho(t)]$, and exact current expression [38], consistent with the Landauer–Büttiker scattering theory [39] and nonequilibrium Green function method [40]. For interacting systems, DEOM converges uniformly and rapidly as the truncated tier L (where $\rho_j^{(n > L)} = 0$) increases, with the required L depending on the specific system-bath configurations [41–45].

Equation (9) constitutes a set of linear differential equations, enabling the use of standard quantum dynamics pictures in the DEOM-space descriptions of open quantum systems [35]. This structure supports consistent DEOM-based evaluations of various physical quantities, including transport current and its correlation function, as outlined below.

C. Transport current and correlation function

The transient current though the lead- α is calculated via $I_{\alpha}(t) = \text{Tr}[\hat{I}_{\alpha} \rho_{\text{tot}}(t)]$, with the current operator $\hat{I}_{\alpha} \equiv -\hat{N}_{\alpha} = -i \sum_u (\hat{a}_u^{\dagger} \hat{F}_{\alpha u}^{-} - \hat{F}_{\alpha u}^{+} \hat{a}_u^{-})$. This leads to

$$I_{\alpha}(t) = -i \sum_{j_{\alpha} \in j} \text{tr}_s[\tilde{a}_{\bar{j}} \rho_j^{(1)}(t)], \quad (11)$$

where $\tilde{a}_{\bar{j}} \equiv \tilde{a}_{\alpha u k}^{\bar{\sigma}} = \bar{\sigma} \hat{a}_u^{\bar{\sigma}}$ and $j_{\alpha} \equiv \{\sigma u k\} \in j \equiv \{\sigma \alpha u k\}$. The current is therefore directly related to the first-tier DDOs.

Similarly, the current-current correlation function can be expressed as

$$\begin{aligned} \langle \hat{I}_{\alpha}(t) \hat{I}_{\alpha'}(0) \rangle & = \text{Tr}[\hat{I}_{\alpha} \rho_{\text{tot}}(t; \hat{I}_{\alpha}')] \\ & = -i \sum_{j_{\alpha} \in j} \text{tr}_s[\tilde{a}_{\bar{j}} \rho_u^{(1)}(t; \hat{I}_{\alpha}')], \end{aligned} \quad (12)$$

which also depends on the first-tier DDOs, but with a different initial condition: $\rho_{\text{tot}}(0; \alpha') = \hat{I}_{\alpha'} \rho_{\text{tot}}^{\text{st}}$, where $\rho_{\text{tot}}^{\text{st}}$ is the steady state of the total system. Using dissipaton-algebra, the initial DDOs are given by

$$\rho_j^{(n)}(0; \alpha') = -i \sum_{j'_{\alpha'} \in j'} \tilde{a}_{\bar{j}'} \rho_{j'j'}^{(n+1); \text{st}} - i \sum_{r=1}^n (-)^{n-r} \tilde{C}_{j_r} \rho_{\bar{j}_r}^{(n-1); \text{st}}.$$

Further details can be found in Refs. [33–35] and numerical applications [46, 47].

The steady-state mean current is denoted by $\bar{I}_\alpha = \langle \hat{I}_\alpha \rangle$ and its fluctuation is given by,

$$\langle \delta \hat{I}_\alpha(t) \delta \hat{I}_{\alpha'}(0) \rangle = \langle [\hat{I}_\alpha(t) - \bar{I}_\alpha][\hat{I}_{\alpha'}(0) - \bar{I}_{\alpha'}] \rangle.$$

The lead-specified noise spectrum is the Fourier transform,

$$S_{\alpha\alpha'}(\omega) = \int_{-\infty}^{\infty} dt e^{i\omega t} \langle \delta \hat{I}_\alpha(t) \delta \hat{I}_{\alpha'}(0) \rangle. \quad (13)$$

Unlike the symmetrized version $S_{\alpha\alpha'}^{\text{sym}}(\omega) = S_{\alpha\alpha'}(\omega) + S_{\alpha\alpha'}(-\omega)$, the asymmetric $S_{\alpha\alpha'}(\omega)$ directly relates to absorption ($\omega > 0$) and ($\omega < 0$) emission processes [48–53]. In this work, we focus on the cross-correlation spectrum $\text{Re}[S_{\text{LR}}(\omega)]$ and its zero-frequency value $S_{\text{LR}}(0) = S_{\text{RL}}(0)$.

III. ISOLATED HYBRIDIZED QD-MZM SYSTEM

In the Fock states basis $\{|n_1 n_M n_2\rangle\}$, the Hamiltonian in Eq. (3) becomes block diagonal. It separates into subspaces of odd parity ($p = -1$), spanned by $\{|100\rangle, |010\rangle, |001\rangle, |111\rangle\}$, and even parity ($p = +1$), spanned by $\{|110\rangle, |000\rangle, |011\rangle, |101\rangle\}$:

$$H_s = \begin{pmatrix} H_- & 0 \\ 0 & H_+ \end{pmatrix}, \quad (14)$$

where the sub-block Hamiltonians are given by

$$H_- = \begin{pmatrix} \varepsilon_1 & \lambda_1 & 0 & \lambda_2 \\ \lambda_1 & \varepsilon_M & \lambda_2 & 0 \\ 0 & \lambda_2 & \varepsilon_2 & \lambda_1 \\ \lambda_2 & 0 & \lambda_1 & \varepsilon_1 + \varepsilon_2 + 2U \end{pmatrix}, \quad (15a)$$

$$H_+ = \begin{pmatrix} \varepsilon_1 + \varepsilon_M + U & \lambda_1 & 0 & \lambda_2 \\ \lambda_1 & 0 & \lambda_2 & 0 \\ 0 & \lambda_2 & \varepsilon_2 + \varepsilon_M + U & \lambda_1 \\ \lambda_2 & 0 & \lambda_1 & \varepsilon_1 + \varepsilon_2 \end{pmatrix}. \quad (15b)$$

Here, we assume the coupling coefficients (λ_1 and λ_2) between the QDs and the MZMs are real, and we set $U_1 = U_2 = U$. In this description of the isolated hybrid QD-MZM system, the parity of H_s is a conserved quantity, since no transitions occur between the two parity subspaces. The focus of the present work is to investigate the effect of Coulomb interaction U on nonlocal behavior in the limit of zero Majorana coupling energy $\varepsilon_M \rightarrow 0$. Therefore, we set $\varepsilon_M = 0$ in the following discussions unless stated otherwise.

A. Noninteracting case: $U = 0$

We first consider the noninteracting case with $U = 0$, where the Hamiltonian satisfies $H_- = H_+$. Starting from

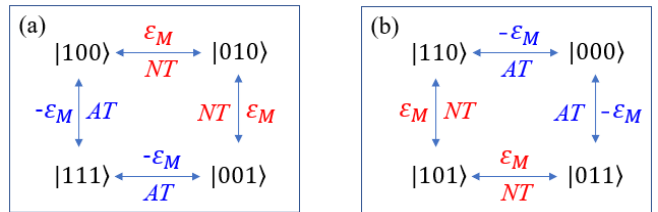


FIG. 2: Coherent electron transitions between the states within the odd-parity subspace (a) and the even-parity subspace (b). The dynamics in each subspace are governed by the Hamiltonian H_- [Eq. (15a)] and H_+ [Eq. (15b)], respectively. Both involve two distinct tunneling processes: normal tunneling (NT) via the electron channel ε_M and anomalous tunneling (AT) via the hole channel $-\varepsilon_M$.

the state $|100\rangle$ (or $|110\rangle$), the quantum evolution is confined to the odd-parity (or even-parity) subspace. The time-dependent occupation probabilities of the electron in the left and the right dots are given by

$$P_1(t) = 1 - \frac{4\lambda_1^2}{\Lambda_1^2} \sin^2(\frac{1}{2}\Lambda_1^2 t), \quad (16a)$$

$$P_2(t) = \frac{4\lambda_2^2}{\Lambda_2^2} \sin^2(\frac{1}{2}\Lambda_2 t), \quad (16b)$$

where $\Lambda_1^2 \equiv \varepsilon_1^2 + 4\lambda_1^2$ and $\Lambda_2^2 \equiv \varepsilon_2^2 + 4\lambda_2^2$. Consistent with previous studies [13, 24], the occupation probabilities of the two dots are independent. For instance, the occupation probability of the right dot does not depend on the coupling strength λ_1 , the energy ε_1 , and the occupation of the left dot. This implies that an electron initially in the left dot cannot be teleported to the right dot—a consequence of destructive interference between the two tunneling channels mediated by the MZMs.

Specifically, $P_2(t)$ can be expressed as the sum of two probabilities, for odd-parity subspace, $P_2(t) = P_{001}(t) + P_{111}(t)$, and for even-parity subspace, and $P_2(t) = P_{011}(t) + P_{101}(t)$. These components are:

$$P_{001}(t) = P_{011}(t) = \frac{4\lambda_1^2 \lambda_2^2}{\Lambda_1^2 \Lambda_2^2} [\cos(\frac{1}{2}\tilde{\Lambda}t) - \cos(\frac{1}{2}\bar{\Lambda}t)]^2, \quad (17a)$$

$$P_{111}(t) = P_{101}(t) = \frac{4\lambda_2^2}{\Lambda_2^2} \sin^2(\frac{1}{2}\Lambda_2 t) - \frac{4\lambda_1^2 \lambda_2^2}{\Lambda_1^2 \Lambda_2^2} [\cos(\frac{1}{2}\tilde{\Lambda}t) - \cos(\frac{1}{2}\bar{\Lambda}t)]^2, \quad (17b)$$

where $\tilde{\Lambda} \equiv \Lambda_1 + \Lambda_2$ and $\bar{\Lambda} \equiv \Lambda_1 - \Lambda_2$. The probabilities in Eq. (17a) and Eq. (17b) arise from the two coherent tunneling channels: normal tunneling (via the electron channel ε_M) and anomalous tunneling (via the hole channel $-\varepsilon_M$), as illustrated in Fig. 2. These two channels become degeneracy when $\varepsilon_M = 0$, leading to quantum destructive interference. In this degenerate limit, the processes contributing to P_{001} and P_{111} (for the odd-parity example) are indistinguishable, resulting in independent dot occupations and vanishing cross-correlations. Lifting this

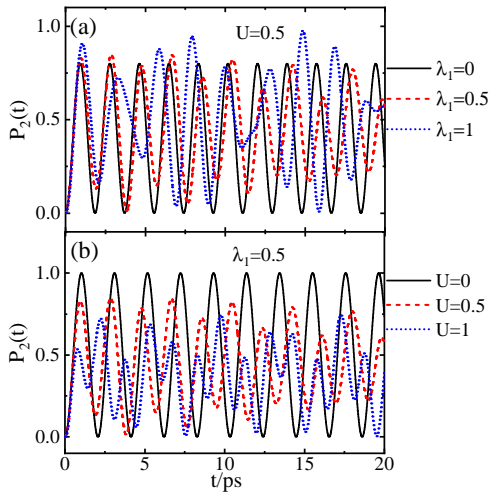


FIG. 3: The time evolution of the occupation probability in the right dot $P_2(t)$ for (a) various λ_1 with $U = 0.5$ and (b) various U for $\lambda_1 = 0.5$. The initial state is $|110\rangle$ with $P_{110}(0) = 1$.

degeneracy makes the combined probabilities $P_{001} + P_{111}$ depend explicitly on λ_1 . Consequently, the occupations of the two dots become correlated, giving rise to nonzero cross correlations and enabling electron transfer between the dots via spatially separated Majorana modes. This teleportation effect was originally proposed in Ref.[25], by taking the large charging energy limit ($E_C \rightarrow \infty$) on the Majorana island, which fully suppresses the AT channel and isolates the NT channel. More recently, Feng *et al.*, [13] demonstrated the effect of finite charging energy E_C to break the degeneracy, yielding nonzero cross correlation in the limit $\varepsilon_M \rightarrow 0$. In the present work, we propose an alternative scheme to remove the degeneracy: introducing finite Coulomb interaction between QDs and the Majorana wire.

B. Interacting case: $U \neq 0$

When Coulomb interaction U is present, the Hamiltonians of odd- and even-parity subspaces are no longer equivalent, i.e., $H_- \neq H_+$, as seen in Eq. (15). In the even-parity subspace described by Eq. (15b), the parameters U and ε_M play similar roles. In contrast, their roles differ in the odd-parity Hamiltonian H_- [Eq. (15a)]: transitions between $|111\rangle$ and $|100\rangle$ (or $|001\rangle$) requires an additional energy $2U$ when proceeding through the AT channel compared to the NT channel, see Fig. 2 (a). Despite this distinction, the underlying physical mechanism is the same—the degeneracy between the two tunneling channels is lifted. This breaking of degeneracy can enable electron teleportation, allowing an electron initially in the left dot can transfer to the right dot via the spatially separated Majorana modes. For clarity, without loss of generality, we further set the energy levels in the

dot as $\varepsilon_1 = \varepsilon_2 = 0$ in the following description.

For the even-parity subspace governed by Eq. (15b), starting from the initial state $|110\rangle$, the time-dependent occupation probabilities of the electron in the left dot and right dot are given by $P_1(t) = P_{110}(t) + P_{101}(t)$ and $P_2(t) = P_{011}(t) + P_{101}(t)$, respectively. Explicitly,

$$P_1(t) = \frac{1}{2} \left[1 + \cos\left(\frac{1}{2}\bar{U}t\right) \cos\left(\frac{1}{2}\tilde{U}t\right) - \frac{4\tilde{\lambda}\bar{\lambda} - U^2}{\tilde{U}\bar{U}} \sin\left(\frac{1}{2}\bar{U}t\right) \sin\left(\frac{1}{2}\tilde{U}t\right) \right], \quad (18a)$$

$$P_2(t) = \frac{1}{2} \left[1 - \cos\left(\frac{1}{2}\bar{U}t\right) \cos\left(\frac{1}{2}\tilde{U}t\right) - \frac{4\tilde{\lambda}\bar{\lambda} + U^2}{\tilde{U}\bar{U}} \sin\left(\frac{1}{2}\bar{U}t\right) \sin\left(\frac{1}{2}\tilde{U}t\right) \right], \quad (18b)$$

where

$$\tilde{U} \equiv \sqrt{U^2 + 4\tilde{\lambda}^2}, \quad \bar{U} \equiv \sqrt{U^2 + 4\bar{\lambda}^2}, \quad (19)$$

with $\tilde{\lambda} = \lambda_1 + \lambda_2$ and $\bar{\lambda} = \lambda_1 - \lambda_2$. Clearly, the charge occupations of the two QDs described by Eq. (18) are mutually dependent. We note that the same expression can be obtained by considering a finite ε_M and replacing U with ε_M in Eq. (18), since the two parameters enter the Hamiltonian H_+ in an analogous manner.

For the odd-parity subspace described by Eq. (15a), analytical solutions are not readily obtainable. We therefore present the numerical results, as shown in Fig. 3. Figure (3a) illustrates that $P_2(t)$ becomes sensitive to λ_1 when U is finite. Moreover, the interaction U modifies both the amplitude and the oscillation frequency of $P_2(t)$ as seen in Fig. 3 (b). These modifications become more pronounced with increasing U , indicating that the nonlocal correlation between the two QDs becomes strengthened as Coulomb interaction grows. Throughout this paper, we set $\lambda_2 = 1(\text{meV})$ as the unit of the energy.

IV. QUANTUM MEASUREMENT

To probe this nonlocal teleportation effect, we examine quantum transport through the QD-MZM hybrid system, as illustrated in Fig. 1. The transport current or conductance can reflect the probability information. Alternatively, one may measure the current noise spectrum—particularly the cross-correlation noise, including its zero-frequency and the finite-frequency components. It is worth noting that, within this transport measurement setup, parity is no longer conserved. Taking again the initial state $|100\rangle$ from the odd-parity subspace as an example, states across the entire Hilbert space—spanning both odd- and even-parity subspaces—will participate in the time evolution due to the tunneling couplings with the two electrodes. After tracing out the freedom of the two electron reservoirs, the QD-MZM hybrid system is described by the reduced system density operator

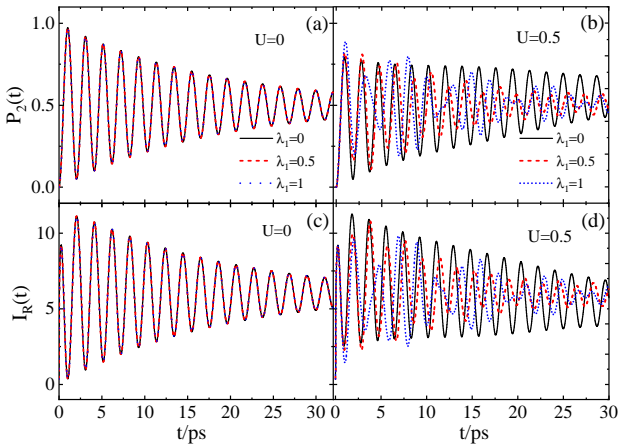


FIG. 4: The time evolution of the occupation probability in the right dot $P_2(t)$, and the transport current through the right electrode $I_R(t)$. (a) For various λ_1 with $U = 0.5$; (b) For various U for $\lambda_1 = 0.5$. The initial state is $|110\rangle$ with $P_{110}(0) = 1$.

$\rho(t) \equiv \text{tr}_B[\rho_{\text{tot}}(t)]$. The exact dynamics of $\rho(t)$ follows the DEOM given by Eq. (9).

In the following numerical calculations, we consider the symmetrical transport configurations with $\Gamma_L = \Gamma_R = \Gamma/2$ and $\mu_L = \mu_R = V/2$, unless specified otherwise. We set $\Gamma = k_B T = 0.1$ and $W = 100$ for wide band reservoirs.

A. The transport current

We examine the transient current in the right electrode $I_R(t)$, using the initial state $|100\rangle$. The numerical results are presented in Fig. 4, where the time evolution of the average current $I_R(t)$ closely follows that of the dot occupation probability $P_2(t)$.

In the absence of the Coulomb interaction ($U = 0$), both $I_R(t)$ and $P_2(t)$ are insensitive to the coupling strength λ_1 , as shown in the left column of Fig. 4. This indicates that the transient currents in the two electrodes [$I_L(t)$ and $I_R(t)$] are independent each other, reflecting the independent occupation probabilities of the right and left QDs. In contrast, when Coulomb interaction is present ($U \neq 0$), both $I_R(t)$ and $P_2(t)$ become distinctly sensitive to λ_1 —a signature of electron teleportation—as displayed in the right column of Fig. 4. These characteristics are fundamentally consistent with the features of the occupation probabilities in the isolated system (without electrodes), discussed in Sec. III and shown in Fig. 3. The primary effect of coupling to the electrodes is to introduce a damped oscillation decay in the occupation dynamics. In a word, the transport current effectively captures the teleportation effect.

Although only the transient current is displayed here, the same behavior applies to the steady-state current, differential conductance, and auto-correlation noise spectrum. All these quantities can reveal the teleportation

phenomena, as they share the same λ_1 -dependence (or lack thereof) in the respective cases with and without the Coulomb interaction. To further explore this nonlocal characteristic, we next investigate the cross-correlation noise spectrum, which provides a more direct and efficient measure of nonlocal correlation, as demonstrated in the following subsection.

B. Cross-correlation noise spectrum

We now examine the current cross-correlation noise spectrum, a widely used tool for probing the non-local behavior [4–13]. Our accurate numerical results are presented in Fig. 5. For $U = 0$, $\text{Re}[S_{\text{LR}}(\omega)] \rightarrow 0$, indicating no correlation between the two QDs. In contrast, for $U \neq 0$, $\text{Re}[S_{\text{LR}}(\omega)]$ exhibits rich structures. Its nonzero value directly reflects the electron teleportation between the two QDs via the Majorana wire. Moreover, the peak-dip features in $\text{Re}[S_{\text{LR}}(\omega)]$ reveal coherent dynamics between the QDs and Majorana wires within each parity subspace. These features occur at characteristic frequencies determined by the energy difference between eigenstates.

For instance, in the even-parity subspace described by Eq. (15b), the eigenenergies are,

$$\begin{aligned} E_1 &= \frac{1}{2}(U - \bar{U}), & E_2 &= \frac{1}{2}(U + \bar{U}), \\ E_3 &= \frac{1}{2}(U - \tilde{U}), & E_4 &= \frac{1}{2}(U + \tilde{U}), \end{aligned} \quad (20)$$

with \tilde{U} and \bar{U} given by Eq. (19). Peak-dip features appear at frequencies $\omega \simeq \pm\Delta_{e1}$ and $\omega \simeq \pm\Delta_{e2}$, where

$$\Delta_{e1} = |E_1 - E_3| = |E_2 - E_4| = \tilde{U} - \bar{U}, \quad (21a)$$

$$\Delta_{e2} = |E_1 - E_4| = |E_2 - E_3| = \tilde{U} + \bar{U}. \quad (21b)$$

Although analytical expressions for the eigenenergies in the odd-parity subspace are not readily obtainable, both parity sectors exhibit similar characteristic frequencies, as confirmed numerically. For the parameters in Fig. 5 (b) with $U = 0.5$, we find $\Delta_{e1} = 0.96$, $\Delta_{o1} \approx 1.14$ and $\Delta_{e2} \sim \Delta_{o2} \approx 2.1$ (indicated by solid arrows). In generally, the correlation signal in $\text{Re}[S_{\text{LR}}(\omega)]$ increases with Coulomb interaction, particularly near zero-frequency. As shown in Fig. 5 (a), $\text{Re}[S_{\text{LR}}(0)] \approx 0.4$ for $U = 1$.

Furthermore, the peak-dip profiles resemble Fano line shapes, indicating interference between the NT and AT channels. If only NT or AT is present, the profiles would reduce to simple peaks or dips. These characteristics are analogous to those observed in double-dot Aharonov-Bohm interferometer [46]. Interestingly, the Fano profiles are only weakly affected by bias voltage, as seen in Fig. 5 (b) when comparing symmetrical ($\mu_L = \mu_R$) and antisymmetrical ($\mu_L = -\mu_R$) bias configurations. However, the zero-frequency response changes dramatically,

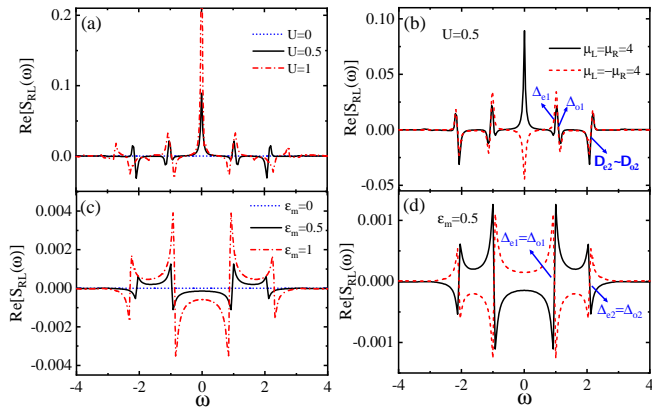


FIG. 5: The cross-correlation noise spectrum $\text{Re}[S_{\text{LR}}(\omega)]$ (in units of $e\lambda_2/\hbar$). In the up panels, we consider $\varepsilon_M = 0$ for (a) different Coulomb interaction U with $\mu_L = \mu_R = 4$, and (b) different chemical potential configurations with $U = 0.5$. For comparison, we also plot the result of $U = 0$ but finite ε_M in the low panels: for (c) different ε_M values, and (d) different chemical potential configurations with $\varepsilon_M = 0.5$.

switching from the positive to negative. Additionally, $\text{Re}[S_{\text{LR}}(0)]$ is larger in the symmetrical case, suggesting that the nonlocal correlation are more easily observed in the zero-frequency component under symmetric biasing.

For comparison, we also examine the effect of the finite Majorana coupling energy ε_M on non-local behavior, as discussed in Ref. [11] for the zero-frequency noise $[S_{\text{LR}}(0)]$. Here, we plot the frequency-dependent correlation noise $\text{Re}[S_{\text{LR}}(\omega)]$ for finite ε_M and $U = 0$ in the lower panels of Fig. 5 [(c) and (d)]. In this case, $H_- = H_+$ for $\varepsilon_1 = \varepsilon_2 = 0$ [Eq. (14)]. The degenerate NT and AT channels split symmetrically around ε_M and $-\varepsilon_M$, respectively (see Fig. 2). The resulting $\text{Re}[S_{\text{LR}}(\omega)]$ displays dip-peak Fano profiles at the eigenfrequencies $\omega \simeq \pm\Delta_{e1} = \pm\Delta_{o1}$ and $\omega \simeq \pm\Delta_{e2} = \pm\Delta_{o2}$ (solid-arrows in Fig. 5 (d)). Upon reversing the bias from symmetric to antisymmetric, the correlated noise exhibits a mirror-image behavior.

Comparing the correlation signal induced by finite Coulomb interaction U [upper panels (a) and (b)] and with that due to finite coupling energy ε_M [lower panels (c) and (d)], we find that the non-local signal in $\text{Re}[S_{\text{LR}}(\omega)]$ arising from U is significantly stronger—about 50 to 100 times larger for the parameters considered. In

practice, ε_M is determined by the length of the Majorana wire. For a topological nanowire with a length of $1\text{--}2\mu\text{m}$ [54], ε_M is at most tens of μeV much smaller than the typical Coulomb interaction U in a QD (on the order of meV [31]). In the topologically relevant long-wire limit, $\varepsilon_M \rightarrow 0$ in general. Therefore, Coulomb interaction between QDs and Majorana wire provides an efficient mechanism for generating nonzero cross correlation.

V. SUMMARY

We have investigated quantum transport in a hybrid QD-MZM system, taking zero Majorana coupling energy ($\varepsilon_M = 0$) to correspond to the topologically relevant long-wire limit. Using the DEOM approach, we accurately evaluated both the transient current and the current-current cross-correlation noise spectrum. Our results demonstrated that the Coulomb interaction between QDs and a Majorana wire provides an efficient mechanism for generating and probing nonlocal electron teleportation mediated by MZMs.

In the absence of interactions, destructive interference between the normal and anomalous tunneling channels suppresses teleportation. As a result, the transport current through the right and left electrodes become independent of each other, yielding a vanishing cross-correlation noise. A finite Coulomb interaction lifts this channel degeneracy, establishing strong nonlocal correlations between the dots. Consequently, the transient current of the right electrode becomes sensitive to the coupling strength between the MZM and left dot. This behavior manifests as a robust, experimentally accessible signal in the cross-correlation noise spectrum—significantly stronger than the signal induced by a finite Majorana coupling energy. Our work highlights Coulomb interaction as a potent and practical control parameter for realizing and detecting Majorana-mediated nonlocal transport in the topologically ideal long-wire limit.

Acknowledgments

We acknowledge helpful discussions with Prof. Xinqi Li. The support from the National Key Research and Development Program of China (Grant No. 2024YFA1408900) is acknowledged.

-
- [1] K. Flensberg, “Tunneling characteristics of a chain of Majorana bound states,” *Phys. Rev. B* **82**, 180516 (2010).
 [2] R. M. Lutchyn, J. D. Sau, and S. Das Sarma, “Majorana Fermions and a Topological Phase Transition in Semiconductor-Superconductor Heterostructures,” *Phys. Rev. Lett.* **105**, 077001 (2010).
 [3] Y. Oreg, G. Refael, and F. von Oppen, “Helical Liquids and Majorana Bound States in Quantum Wires,” *Phys.*

- Rev. Lett.* **105**, 177002 (2010).
 [4] K. T. Law, P. A. Lee, and T. K. Ng, “Majorana Fermion Induced Resonant Andreev Reflection,” *Phys. Rev. Lett.* **103**, 237001 (2009).
 [5] J. Liu, F.-C. Zhang, and K. T. Law, “Majorana fermion induced nonlocal current correlations in spin-orbit coupled superconducting wires,” *Phys. Rev. B* **88**, 064509 (2013).
 [6] J. Ulrich and F. Hassler, “Majorana-assisted nonlocal

- electron transport through a floating topological superconductor,” *Phys. Rev. B* **92**, 075443 (2015).
- [7] C. J. Bolech and E. Demler, “Observing Majorana bound States in p -Wave Superconductors Using Noise Measurements in Tunneling Experiments,” *Phys. Rev. Lett.* **98**, 237002 (2007).
- [8] J. Nilsson, A. R. Akhmerov, and C. W. J. Beenakker, “Splitting of a Cooper Pair by a Pair of Majorana Bound States,” *Phys. Rev. Lett.* **101**, 120403 (2008).
- [9] B. Zocher and B. Rosenow, “Modulation of Majorana-Induced Current Cross-Correlations by Quantum Dots,” *Phys. Rev. Lett.* **111**, 036802 (2013).
- [10] B. Zocher and B. Rosenow, “Modulation of Majorana-Induced Current Cross-Correlations by Quantum Dots,” *Phys. Rev. Lett.* **111**, 036802 (2013).
- [11] H.-F. Lü, H.-Z. Lu, and S.-Q. Shen, “Current noise cross correlation mediated by Majorana bound states,” *Phys. Rev. B* **90**, 195404 (2014).
- [12] H.-F. Lü, H.-Z. Lu, and S.-Q. Shen, “Enhanced current noise correlations in a Coulomb-Majorana device,” *Phys. Rev. B* **93**, 245418 (2016).
- [13] W. Feng, L. Qin, and X.-Q. Li, “Cross correlation mediated by Majorana island with finite charging energy,” *New Journal of Physics* **23**, 123032 (2021).
- [14] V. Mourik, K. Zuo, S. M. Frolov, S. R. Plissard, E. P. A. M. Bakkers, and L. P. Kouwenhoven, “Signatures of Majorana Fermions in Hybrid Superconductor-Semiconductor Nanowire Devices,” *Science* **336**, 1003 (2012).
- [15] M. T. Deng, C. L. Yu, G. Y. Huang, M. Larsson, P. Caroff, and H. Q. Xu, “Anomalous Zero-Bias Conductance Peak in a Nb-InSb Nanowire-Nb Hybrid Device,” *Nano Lett.* **12**, 6414 (2012).
- [16] A. Das, Y. Ronen, Y. Most, Y. Oreg, M. Heiblum, and H. Shtrikman, “Zero-bias peaks and splitting in an Al-InAs nanowire topological superconductor as a signature of Majorana fermions,” *Nat. Phys.* **8**, 887 (2012).
- [17] A. D. K. Finck, D. J. Van Harlingen, P. K. Mohseni, K. Jung, and X. Li, “Anomalous Modulation of a Zero-Bias Peak in a Hybrid Nanowire-Superconductor Device,” *Phys. Rev. Lett.* **110**, 126406 (2013).
- [18] S. M. Albrecht, A. P. Higginbotham, M. Madsen, F. Kuemmeth, T. S. Jespersen, J. Nygård, P. Krogstrup, and C. M. Marcus, “Exponential protection of zero modes in Majorana islands,” *Nature* **531**, 206 (2016).
- [19] A. Y. Kitaev, “Unpaired Majorana fermions in quantum wires,” *Physics-Uspekhi* **44**, 131 (2001).
- [20] A. Kitaev, “Fault-tolerant quantum computation by anyons,” *Annals of Physics* **303**, 2 (2003).
- [21] C. Nayak, S. H. Simon, A. Stern, M. Freedman, and S. Das Sarma, “Non-Abelian anyons and topological quantum computation,” *Rev. Mod. Phys.* **80**, 1083 (2008).
- [22] M. Leijnse and K. Flensberg, “Quantum Information Transfer between Topological and Spin Qubit Systems,” *Phys. Rev. Lett.* **107**, 210502 (2011).
- [23] G. W. Semenoff and P. Sodano, “Stretched quantum states emerging from a Majorana medium,” *Journal of Physics B: Atomic, Molecular and Optical Physics* **40**, 1479 (2007).
- [24] S. Tewari, C. Zhang, S. Das Sarma, C. Nayak, and D.-H. Lee, “Testable Signatures of Quantum Nonlocality in a Two-Dimensional Chiral p -Wave Superconductor,” *Phys. Rev. Lett.* **100**, 027001 (2008).
- [25] L. Fu, “Electron Teleportation via Majorana Bound States in a Mesoscopic Superconductor,” *Phys. Rev. Lett.* **104**, 056402 (2010).
- [26] Z. Wang, X.-Y. Hu, Q.-F. Liang, and X. Hu, “Detecting Majorana fermions by nonlocal entanglement between quantum dots,” *Phys. Rev. B* **87**, 214513 (2013).
- [27] S. Plugge, A. Zazunov, P. Sodano, and R. Egger, “Majorana entanglement bridge,” *Phys. Rev. B* **91**, 214507 (2015).
- [28] V. K. Vimal and J. Cayao, “Entanglement measures of Majorana bound states,” *Phys. Rev. B* **110**, 224510 (2024).
- [29] C. Jasiukiewicz, A. Sinner, I. Weymann, T. Domański, and L. Chotorlishvili, “Entanglement between quantum dots transmitted via a Majorana wire: Insights from the fermionic negativity, concurrence, and quantum mutual information,” *Phys. Rev. B* **111**, 075415 (2025).
- [30] S. Walter and J. C. Budich, “Teleportation-induced entanglement of two nanomechanical oscillators coupled to a topological superconductor,” *Phys. Rev. B* **89**, 155431 (2014).
- [31] L. S. Ricco, Y. Marques, J. E. Sanches, I. A. Shelykh, and A. C. Seridonio, “Interaction induced hybridization of Majorana zero modes in a coupled quantum-dot-superconducting-nanowire hybrid system,” *Phys. Rev. B* **102**, 165104 (2020).
- [32] H.-F. Lü, H.-Z. Lu, and S.-Q. Shen, “Nonlocal noise cross correlation mediated by entangled Majorana fermions,” *Phys. Rev. B* **86**, 075318 (2012).
- [33] Y. J. Yan, “Theory of open quantum systems with bath of electrons and phonons and spins: Many-dissipaton density matrixes approach,” *J. Chem. Phys.* **140**, 054105 (2014).
- [34] J. S. Jin, S. K. Wang, X. Zheng, and Y. J. Yan, “Current noise spectra and mechanisms with dissipaton equation of motion theory,” *J. Chem. Phys.* **142**, 234108 (2015).
- [35] Y. J. Yan, J. S. Jin, R. X. Xu, and X. Zheng, “Dissipaton equation of motion approach to open quantum systems,” *Frontiers Phys.* **11**, 110306 (2016).
- [36] J. Hu, R. X. Xu, and Y. J. Yan, “Padé spectrum decomposition of Fermi function and Bose function,” *J. Chem. Phys.* **133**, 101106 (2010).
- [37] J. Hu, M. Luo, F. Jiang, R. X. Xu, and Y. J. Yan, “Padé spectrum decompositions of quantum distribution functions and optimal hierarchical equations of motion construction for quantum open systems,” *J. Chem. Phys.* **134**, 244106 (2011).
- [38] J. S. Jin, X. Zheng, and Y. J. Yan, “Exact dynamics of dissipative electronic systems and quantum transport: Hierarchical equations of motion approach,” *J. Chem. Phys.* **128**, 234703 (2008).
- [39] S. Datta, *Electronic Transport in Mesoscopic Systems*, Oxford University Press, New York, 1995.
- [40] H. Haug and A.-P. Jauho, *Quantum Kinetics in Transport and Optics of Semiconductors*, Springer-Verlag, Berlin, 2nd, substantially revised edition, 2008, Springer Series in Solid-State Sciences 123.
- [41] X. Zheng, R. X. Xu, J. Xu, J. S. Jin, J. Hu, and Y. J. Yan, “Hierarchical equations of motion for quantum dissipation and quantum transport,” *Prog. Chem.* **24**, 1129 (2012).
- [42] Z. H. Li, N. H. Tong, X. Zheng, D. Hou, J. H. Wei, J. Hu, and Y. J. Yan, “Hierarchical Liouville-space approach for accurate and universal characterization of quantum

- impurity systems,” *Phys. Rev. Lett.* **109**, 266403 (2012).
- [43] X. Zheng, Y. J. Yan, and M. Di Ventra, “Kondo memory in driven strongly correlated quantum dots,” *Phys. Rev. Lett.* **111**, 086601 (2013).
- [44] D. Hou, S. K. Wang, R. L. Wang, L. Z. Ye, R. X. Xu, X. Zheng, and Y. J. Yan, “Improving the efficiency of hierarchical equations of motion approach and application to coherent dynamics in Aharonov–Bohm interferometers,” *J. Chem. Phys.* **142**, 104112 (2015).
- [45] L. Z. Ye, X. L. Wang, D. Hou, R. X. Xu, X. Zheng, and Y. J. Yan, “HEOM-QUICK: A program for accurate, efficient and universal characterization of strongly correlated quantum impurity systems,” *WIREs Comp. Mol. Sci.* **6**, 608 (2016).
- [46] J. S. Jin, “Nonequilibrium noise spectrum and Coulomb blockade assisted Rabi interference in a double-dot Aharonov–Bohm interferometer,” *Phys. Rev. B* **101**, 235144 (2020).
- [47] H. Mao, J. Jin, S. Wang, and Y. Yan, “Nonequilibrium Kondo regime current noise spectrum of quantum dot systems with the single impurity Anderson model,” *The Journal of Chemical Physics* **155**, 014104 (2021).
- [48] H.-A. Engel and D. Loss, “Asymmetric quantum shot noise in quantum dots,” *Phys. Rev. Lett.* **93**, 136602 (2004).
- [49] E. A. Rothstein, O. Entin-Wohlman, and A. Aharony, “Noise spectra of a biased quantum dot,” *Phys. Rev. B* **79**, 075307 (2009).
- [50] P.-Y. Yang, C.-Y. Lin, and W.-M. Zhang, “Transient current-current correlations and noise spectra,” *Phys. Rev. B* **89**, 115411 (2014).
- [51] J. Basset, H. Bouchiat, and R. Deblock, “Emission and absorption quantum noise measurement with an on-chip resonant circuit,” *Phys. Rev. Lett.* **105**, 166801 (2010).
- [52] J. Basset, A. Y. Kasumov, C. P. Moca, G. Zaránd, P. Simon, H. Bouchiat, and R. Deblock, “Measurement of quantum noise in a carbon nanotube quantum dot in the Kondo regime,” *Phys. Rev. Lett.* **108**, 046802 (2012).
- [53] R. Delagrangé, J. Basset, H. Bouchiat, and R. Deblock, “Emission noise and high frequency cut-off of the Kondo effect in a quantum dot,” *Phys. Rev. B* **97**, 041412 (2018).
- [54] S. Das Sarma, J. D. Sau, and T. D. Stanescu, “Splitting of the zero-bias conductance peak as smoking gun evidence for the existence of the Majorana mode in a superconductor-semiconductor nanowire,” *Phys. Rev. B* **86**, 220506 (2012).